Dyes and Pigments 99 (2013) 41–51

Contents lists available at SciVerse ScienceDirect

Dyes and Pigments

journal homepage: www.elsevier.com/locate/dyepig

Bipolar iridium dendrimers containing carbazolyl dendron and 1,2,4-triazole unit for solution-processed saturated red electrophosphorescence

Bo Liang [a,*], Sujun Hu [b], Yanping Liu [a], Zhiqiang Fan [a], Xueye Wang [c], Weiguo Zhu [c], Hongbin Wu [b], Yong Cao [b]

[a] Department of Material Forming and Control Engineering, School of Automobile and Mechanic Engineering, Changsha University of Science & Technology, Changsha 410076, PR China
[b] Institute of Polymer Optoelectronic Materials and Devices, State Key Laboratory of Luminescent Materials and Devices, South China University of Technology, Guangzhou 510640, PR China
[c] College of Chemistry, Key Lab of Environment-Friendly Chemistry and Application of Ministry of Education, Xiangtan University, Xiangtan 411105, PR China

ARTICLE INFO

Article history:
Received 13 January 2013
Received in revised form
15 April 2013
Accepted 16 April 2013
Available online 24 April 2013

Keywords:
Dendrimer
Bipolar transport
Iridium complex
Host-free OLEDs
Electrophosphorescent devices
Solution-process

ABSTRACT

Two solution-processable, carbazole-based iridium dendrimers (**Ir-1** and **Ir-2**) were synthesized and characterized. The presence of carbazolyl substituent on the cyclometallated ligand resulted in improved solubility, good control over intermolecular interactions, and improved hole transport properties. The triazole ancillary ligand led to improved electron transport properties. When the dendrimers were employed as host-free light-emitting layers in the OLEDs, the devices exhibited a low turn-on voltage of 5.4 V. The maximal external quantum efficiencies and luminous efficiency of the devices obtained from **Ir-1** and **Ir-2** were 5.1% and 3.3 cd A^{-1} and 7.9% and 4.4 cd A^{-1}, respectively, both with saturated red emission (CIE coordinates, 0.663, 0.332). The devices have a structure of indium tin oxide/poly(3,4-ethylenedioxythiophene)/dendrimer/1,3,5-tris(N-phenylbenzimiazole-2-yl)benzene/cesium fluoride/aluminum. Given ease of synthesis and good device performance, these iridium dendrimers can be used to fully exploit the potential of low-cost OLEDs, leading to more applications in high-efficiency OLEDs.

1. Introduction

Organic light-emitting diodes (OLEDs) have drawn intensive attention given their potential applications in flat panel displays and solid-state lighting sources [1–3]. Materials and devices based on heavy metal complexes have been extensively investigated because of their high efficiency (up to 100% for internal quantum efficiency (IQE) because of the harvest of singlet and triplet excitons) and tunable emission color in the entire visible region, as determined by ligand modification [4]. Electrophosphorescent devices based on Ir(III) complexes are typically fabricated by blending these dopants into a host with an appropriately wide bandgap, such as that derived in small molecules treated via thermal evaporation under high vacuum [5,6] or polymer hosts subjected to solution mixing and subsequent spin coating [7–9]. The host materials used for carrier transport or carrier blocking must have sufficiently high triplet energy to prevent the loss of triplet excitons from metal complexes [10]. The average separation of the chromophores can be readily tuned by molecular structures and multilayer device configurations [11,12]. Yang et al. reported highly efficient solution-processed green and red electrophosphorescent devices enabled by a small-molecule bipolar host that comprises hole-transporting triphenylamine and electron-transporting oxadiazole; the efficiency of the green light-emitting device was elevated to 56.8 cd A^{-1} [13]. Although significant success in bipolar host-based OLEDs has been achieved, doping with electron-transporting or hole-transporting materials in a host–guest blend remains the primary approach to obtaining high-performance OLEDs. However, the blend system usually suffers from phase separation problems. Phosphorescent OLEDs consist of multiple layers for charge carriers balancing and exciton confinement [14,15], which may limit their practical applications.

Solution-processed phosphorescent dendrimers (containing an emitting core, dendrons, and a surface group) serve as an alternative promising approach to realizing high-performance, low-cost, and large-area OLEDs [16]. Dendrons are generally attached to cores

* Corresponding author. Tel./fax: +86 731 85258630.
E-mail address: liangbo26@126.com (B. Liang).

0143-7208/$ – see front matter © 2013 Elsevier Ltd. All rights reserved.
http://dx.doi.org/10.1016/j.dyepig.2013.04.020

and act as spacers that control the interactions between the cores and endow OLEDs with charge transport properties [17,18]. Samuel et al. developed green phosphorescent dendrimers containing fac-tri(2-phenylpyridyl)iridium(III) cores, biphenyl-based dendrons, and 2-ethylhexyloxy surface groups, and found that charge transport occurs via hopping between the electroactive cores [19–21]. Higher generation materials have favorable photophysical properties, but reduced charge mobility [22,23]. The performance of a device is considerably influenced by the charge balance from opposite electrodes; thus, a highly desirable solution is to design phosphorescent dendrimers with enhanced charge balance features that enable complete transfer of energy between host and dopant molecules [24,25]. An effective method for controlling the interactions between the cores of these dendrimers is to increase the number of dendrons close to the core, forming "double dendron" materials. This method demonstrates that efficient photoluminescence (PL) and electroluminescence (EL) can be readily obtained from neat films [26,27]. Wang et al. developed bifunctional electrophosphorescent green light-emitting devices by increasing the density of carbazole dendrons at the edge of the emissive core, in which the core acts as the emissive dopant and the dendron serves as the host [28]. Wong et al. reported homogeneous red light-emitting dendrimers with triphenylamine as dendrimer, showing a bathochromic shift from pure red at 620 nm to saturated red at 641 nm in dichloromethane with increased generation from G0 to G2 [29].

In our previous work, we designed and successfully synthesized a series of red dendrimers by incorporating an energy transfer-favorable ancillary ligand with 2-pyridyltriazole. The introduction of the 1,2,4-triazole group into the ancillary ligand can lead to a blue shift of the emitted color as a result of enabled Förester energy transfer from the singlet-excited state in the host to the metal-to-ligand charge transfer (MLCT) band of the guest [30,31]. To simplify the device structure by using an emitter with charge transport capability, we report the synthesis and characterization of two dendritic cyclometalated iridium(III) complexes. The complexes contain three 3, 6-dicarbazole groups or three 9-phenyl carbazole units between the iridium centers as spacers and a triazole compound as the ancillary ligand, which enable the dendrimers to perform bipolar transport. As strong electron-withdrawing groups, 1,2,4-triazole derivatives can enhance electron withdrawal capabilities, thereby reducing the lowest unoccupied molecular orbital (LUMO) level and increasing the highest occupied molecular orbital (HOMO)–LUMO gap [32]. The triazole group can compensate for the bathochromic shift from the large conjugated dendritic group, enabling saturated red emission. Compared with the corresponding devices from the blend system, those with host-free structures exhibited improved performance, indicating that excellent solution-processing properties, charge transport properties, and electrophosphorescent performance are combined in the carefully designed iridium dendrimers. These materials can serve as a new route to synthesizing metal phosphors with optimized electroluminescent efficiency/color purity tradeoff for pure red emission.

2. Experiments

2.1. Measurement and characterization

2.1.1. Materials

All reagents and solvents, unless otherwise specified, were obtained from Aldrich, Acros, and TCI Chemical Co. and were used as received. All manipulations involving air-sensitive reagents were performed under a dry argon atmosphere. Anhydrous tetrahydrofuran was distilled over sodium/benzophenone under N_2 prior to use. 3-Bromo-N-phenethyl benzamide (**1**), 1-(3-bromo phenyl)-3,4-dihydroisoquinoline (**2**), N-(4-bromophenyl)carbazole (**3**), N-(4-(4,4,5,5-tetramethyl-1,3,2-dioxaborolan-2′-yl)phenyl)carbazole (**4**) [30], 3-Bromocarbazole (**8**), 3-bromo-N-(2-ethylhexyl) carbazole (**9**), and 3-(4,4,5,5-tetramethyl-1,3,2-dioxaborolan-2-yl)-N-(2-ethylhexyl)carbazole (**10**) [33] were synthesized in a similar manner as published procedures. Tetrabutylammonium hexafluorophosphate (Bu_4NPF_6) was recrystallized from a 50:50 mixture of methanol/water and dried at 60 °C under vacuum.

2.1.2. Instrumentation

^1H NMR spectra were recorded on a Bruker AV 300 spectrometer with tetramethylsilane as the internal reference. The molecular weights of the compounds were obtained on a Trace 2000 Series (CE Instruments Company) or Voyager DEPRO matrix-assisted laser desorption-ionization time-of-flight (MALDI-TOF) spectrometer (Applied Biosystems). Elemental analyses were performed on a Vario EL elemental analysis instrument (Elementar Co.). UV–vis absorption spectra were recorded on an HP 8453 spectrophotometer. Cyclic voltammetry (CV) was carried out on a CHI660A electrochemical workstation with platinum electrodes at a scan rate of 50 mV/s against a saturated calomel reference electrode (SCE) with an argon-saturated solution of 0.1 M tetrabutylammonium hexafluorophosphate (Bu_4NPF_6) in dichloromethane (CH_2Cl_2). Atomic force microscopy (AFM) images were obtained with a Nanoscope IIIa instrument (Digital Instruments) in tapping mode. A crystal silicon tip with a resonant frequency of 300–350 kHz and a spring constant of 20–100 N/m was used. The scanner was a 10 μm piezo scanner with a scan rate of 1–2 Hz. Offline image processing and analysis (grain size, roughness) were performed using DI offline software (Veeco Corp).

2.1.3. Computational method

The geometric optimization and energy level calculation of the ground state of the ligands were obtained by the Becke–Lee–Young–Parr composite exchange correlation functional [34] method with the 6–31G basis set. Calculations of the electronic ground states of the Ir (III) dendrimers were conducted using the same calculation method, except for the LANL2DZ [35] basis set for the Ir atom. All of the calculations were accomplished by density functional theory (DFT) [36] methods using the Gaussian 03 software package [37] in vacuo without any constrained symmetry. Accomplishing the solvent effect computations was difficult because of the large systems and the condition of our equipment.

2.1.4. Device fabrication and characterization

A patterned indium tin oxide (ITO)-coated glass with a sheet resistance of 15 Ω/square was cleaned by a surfactant scrub and then subjected to a wet-cleaning process in an ultrasonic bath, beginning with deionized water followed by acetone and isopropanol. The thicknesses of the poly(3,4-ethylendioxythiophene) (PEDOT): poly(styrenesulfonate) (PSS) and active layer were verified by a surface profilometer (Tencor, Alpha-500). A layer of PEDOT (60 nm) was spin-cast onto pre-cleaned ITO-glass substrates. Then, a 40 nm-thick layer of poly(vinylcarbazole) (PVK) was spin-cast onto the top of PEDOT. The iridium dendrimers were then spin-coated from a chlorobenzene solution (30 mg/mL) to yield an 80-nm thick dense layer of either **Ir-1** or **Ir-2**. To determine the factors that limit device efficiency and improve device performance, an electron-transporting layer of 1,3,5-tris(2-N-phenylbenzimidazolyl)benzene (TPBI) with a thickness of 60 nm was used. Cesium fluoride (CsF) (1 nm) and aluminum (Al) (80 nm) were used as electron-injection layer and cathode. The thickness of the evaporated cathodes was monitored by a quartz crystal thickness/ratio

monitor (model: STM-100/MF, Sycon). Except for the deposition of the PEDOT:PSS layers, all the fabrication processes were conducted in a controlled nitrogen dry box atmosphere (Vacuum Atmosphere Co.). The current density–luminance–voltage (*J–L–V*) characteristics were measured using a Keithley 236 source measurement unit and a calibrated silicon photodiode. The luminance was calibrated using a spectrophotometer (Photo Research, Model: SpectraScan PR-705). Absolute photoluminescent efficiencies were measured in an integrating sphere (IS-080, Labsphere) under 325 nm line of HeCd laser. External electroluminescent quantum efficiencies (QE) were obtained by measuring the total light output in all directions in the integrating sphere. The external quantum efficiency (EQE) of the device was collected by measuring the total light output in all directions in the integrating sphere. PL and EL spectra were recorded using a charge-coupled device spectrophotometer (Instaspec 4, Oriel).

2.2. Synthesis

The synthetic routes of the ligands and iridium dendrimers are shown in Schemes 1 and 2.

2.2.1. 1-(3-(N-carbazolyl)biphenyl)-3, 4-dihydoisoquinoline (**5**)

The solution of 6.50 g (22.7 mmol) **2,** 9.22 g (25.0 mmol) **4,** 12.6 mL of 2 M sodium carbonate, 70 mL of toluene, and 35 mL of ethanol were degassed with argon for 20 min, and then 0.578 g $Pd(PPh_3)_4$ was added. The solution was refluxed for 24 h under argon. After cooling to room temperature, 10 mL of water was added. The aqueous layer was extracted with dichloromethane and dried with anhydrous magnesium sulfate. The product was purified by silica-gel column chromatography using ethyl acetate/dichloromethane (1/9) as the eluent and dried in vacuum to yield a yellow powder (8.22 g, 80.6%). Gas chromatography–mass

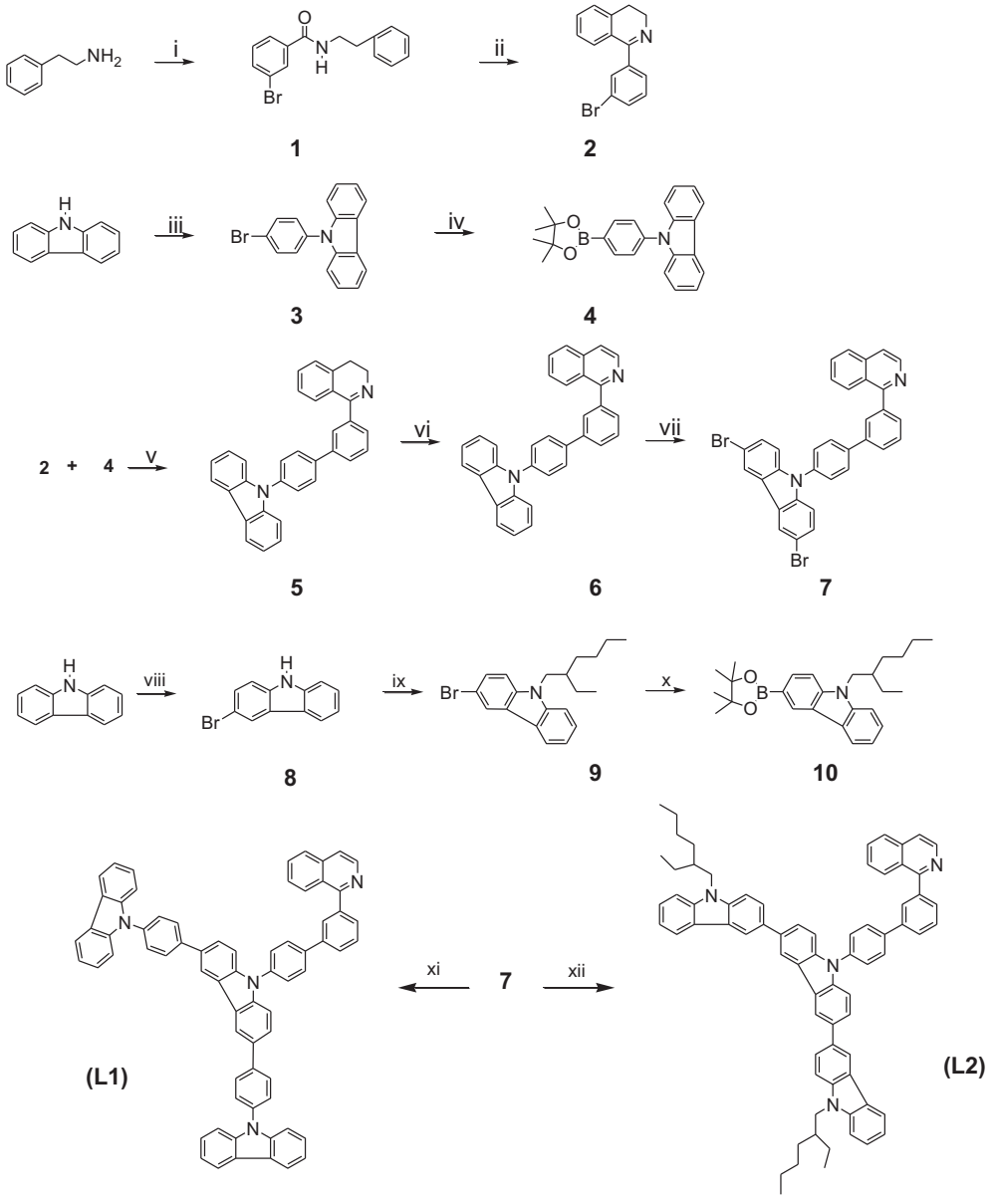

Scheme 1. Synthetic route for the ligands. Reagents and conditions: (i) 3-bromobenzoyl chloride, Et_3N, CH_2Cl_2; (ii) xylene, P_2O_5, $POCl_3$; (iii) 4-bromoiodobenzene, 1,10-phenanthroline, CuCl, anhydrous KOH, xylene, Ar; (iv) THF, *n*-BuLi, 2-isopropoxy-4,4,5,5-tetramethyl-1,3,2-dioxaborolane; (v) $Pd(PPh_3)_4$, 2 mol/L Na_2CO_3, toluene:ethanol = 2:1, Ar; (vi) 10% Pd/C, mesitylene, Ar; (vii) NBS, $CHCl_3$; (viii) NBS, $CHCl_3$; (ix) *t*-BuOK, 1-Bromo-2-ethyl hexane; (x) THF, *n*-BuLi, 2-isopropoxy-4,4,5,5-tetramethyl-1,3,2-dioxaborolane; (xi) **4**, $Pd(PPh_3)_4$, 2 mol/L Na_2CO_3, toluene:ethanol = 2:1, Ar; (xii) **10**, $Pd(PPh_3)_4$, 2 mol/L Na_2CO_3, toluene:ethanol = 2:1, Ar.

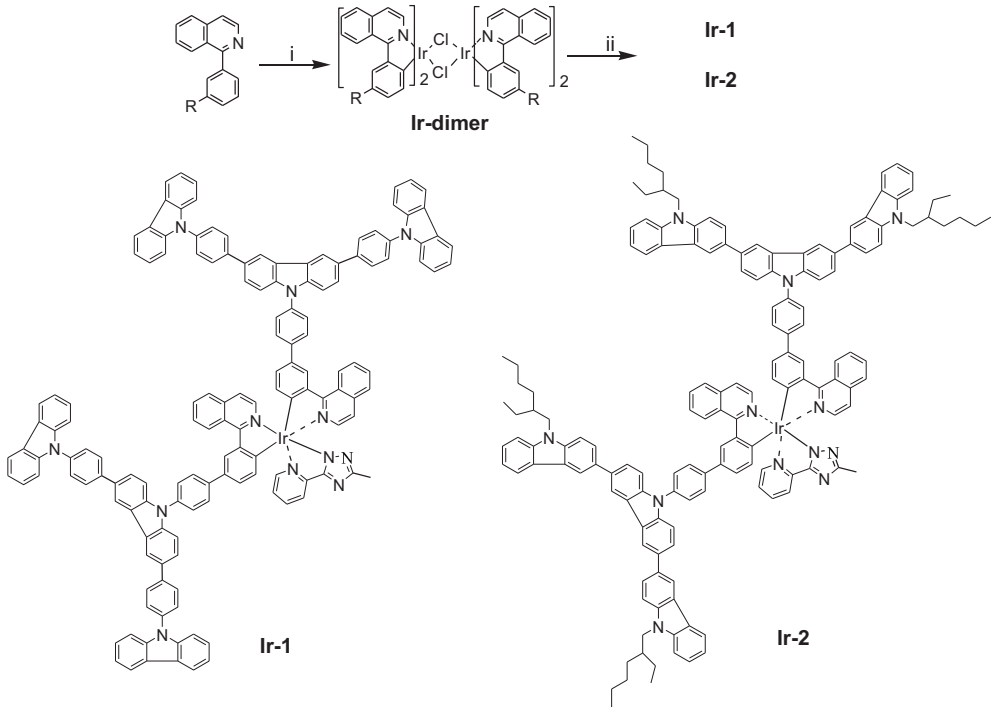

Scheme 2. Synthetic route for the iridium complexes dendrimers. Reagents and conditions: (i) $IrCl_3.3H_2O$, 2-ethoxylethanol/H_2O (3/1), 120 °C; (ii)$NaOCH_3$, ethanol, 50 °C, 5-methyl-3-(pyridin-2′-yl)-1*H*-1,2,4-triazole, refluxed 3–5 h.

spectrometry (GC–MS): *m*/*z*, 447.2, $[M - 1]^+$. ^1H NMR (300 MHz, $CDCl_3$), (ppm): 8.17–8.14 (d, 2H), 7.96 (s, 1H), 7.88–7.85 (m, 2H), 7.81–7.78 (m, 1H), 7.66–7.55 (m, 4H), 7.48–7.40 (m, 6H), 7.36–7.27 (m, 4H), 3.94–3.89 (m, 2H), 2.89–2.85 (t, 2H).

*2.2.2. 1-(3-(N-carbazolyl)biphenyl)lisoquinoline (**6**)*

Up to 3.52 g (7.86 mmol) **5** was dissolved in 20 mL mesitylene, and then 0.45 g 10% Pd/C was added. The solution was refluxed for 3 h at 190 °C under argon. After cooling to room temperature, the solution was filtered and the black powder was washed with dichloromethane several times. The product was purified by recrystallization from petroleum ether, and dried to yield a pale powder (3.09 g, 88.2%). GC–MS: *m*/*z*, 445.2, $[M - 1]^+$. ^1H NMR (300 MHz, $CDCl_3$) (ppm): 8.68–8.67 (m, 1H), 8.22–8.14 (m, 3H), 8.04 (s, 1H), 7.96–8.83 (m, 4H), 7.83–7.58 (m, 7H), 7.49–7.39 (m, 4H), 7.32–7.27 (m, 2H).

*2.2.3. 1-(3-(N-(3, 6-dibromocarbazolyl)))biphenylisoquinoline (**7**)*

Up to 2.45 g (5.49 mmol) **6** was dissolved in 20 mL chloroform, and then 1.98 g (11.12 mmol) N-bromosuccinimide in chloroform was added dropwise to the solution, which was then stirred at room temperature for 3 h. The product was purified by silica-gel column chromatography using ethyl acetate/dichloromethane (1/9) as the eluent to yield a yellow powder (2.83 g, 85.8%). Electrospray ionization–MS: *m*/*z*, 605.0, $[M + 1]^+$. ^1H NMR (300 MHz, $CDCl_3$), (ppm): 8.67–8.65 (d, 1H), 8.20–8.18 (d, 3H), 8.02 (s, 1H), 7.94–7.88 (m, 3H), 7.85–7.62 (m, 4H), 7.58–7.50 (m, 5H), 7.32–7.26 (m, 2H).

2.2.4. Synthesis of L1

Up to 0.909 g (1.5 mmol) **7**, 1.12 g (3.0 mmol) **4**, and 3 mL of 2 M sodium carbonate solution were added to the solvent containing 30 mL toluene and 15 mL ethanol. After degassing with argon, 0.069 g $Pd(PPh_3)_4$ was added. The mixture was refluxed for 24 h under argon, and then 10 mL water was added after the solution

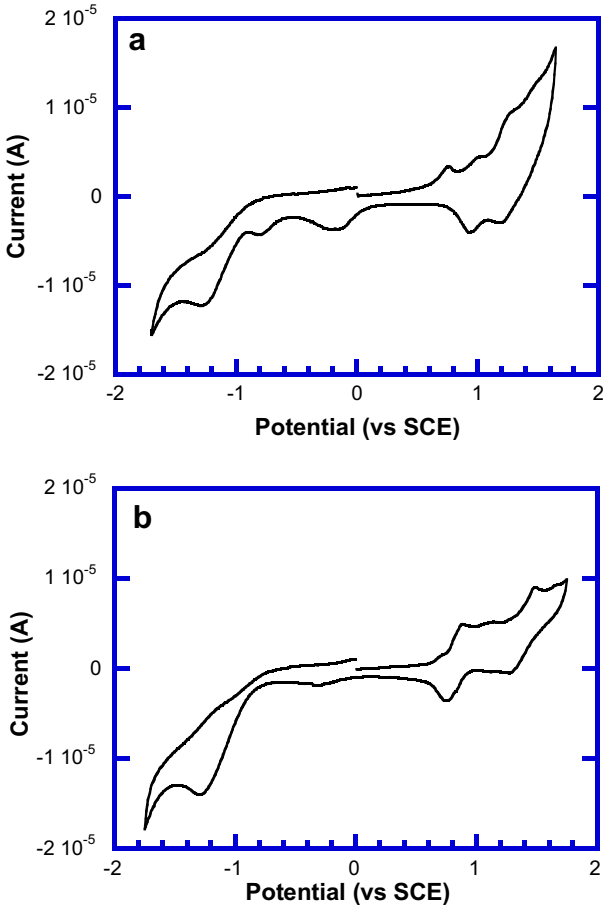

Fig. 1. Cyclic voltammograms of **Ir-1**(a), **Ir-2**(b) (scan rate: 50 mV/s, solvent: CH_2Cl_2).

Table 1
The optical and electrochemical properties of the complexes.

Complexes	E_{ox}[b] (V)	E_{red}[b] (V)	HOMO[c] (ev)	LUMO[c] (ev)	E_{gap} (ev)	UV[d] (nm)	PL (nm)[d]	PL efficiency[e] (%)
G0[a]	0.97	−1.44	−5.37	−2.96	2.41	233, 293 353, 455	593	3.3
Ir-1	0.56, 0.88, 1.10	−1.49	−4.96	−2.91	2.05	240, 294, 315	604	7.83
Ir-2	0.70, 1.05, 1.26	−1.46	−5.10	−2.94	2.16	246, 277, 306	606	10.65

Measurement detailed:
[a] Data from Ref. [30].
[b] Quasi-reversible or irreversible; E_{ox} and E_{red} are the onset potential of oxidation and reduction, respectively.
[c] Calculated from the empirical formula, $E_{(HOMO)} = -(E_{ox} + 4.40)$ (eV), $E_{(LUMO)} = -(E_{red} + 4.40)$ (eV).
[d] The UV and PL data was obtained in CH_2Cl_2 solution.
[e] Measured in integrating sphere under 325 nm line of HeCd laser.

cooled. The aqueous layer was extracted with dichloromethane three times and dried with anhydrous magnesium sulfate. The product was purified by silica-gel column chromatography using dichloromethane/petroleum ether (1/9) as the eluent and dried in vacuum to yield a white powder (1.03 g, 73.9%). MALDI-TOF: MH^+, 929.5 (100%), ^{1}H NMR ($CDCl_3$, 300 MHz), (ppm): 8.69–8.67 (d, 1H), 8.54 (s, 2H), 8.23–8.05 (m, 6H), 7.96–7.92 (m, 7H), 7.78–7.63 (m, 11H), 7.60–7.56 (m, 2H), 7.52–7.31 (m, 8H), 7.34–7.20 (m, 7H). ^{13}C NMR ($CDCl_3$, 75 MHz): δ (ppm) 149.52, 146.63, 142.19, 140.52, 138.00, 130.69, 130.27, 130.16, 128.90, 128.69, 127.52, 127.35, 127.12, 126.73, 126.07, 125.91, 124.42, 123.97, 123.66, 123.38, 122.89, 122.65, 121.11, 119.48, 118.74, 113.47.

2.2.5. Synthesis of L2

Up to 0.909 g (1.5 mmol) **7**, 1.34 g (3.3 mmol) **10**, and 3 mL of 2 M sodium carbonate solution were added to the solvent containing 30 mL toluene and 15 mL ethanol. Synthesis details are similar to those described for **L1** (1.28 g, 85.2%). MALDI-TOF: MH^+, 1000.6 (100%), ^{1}H NMR ($CDCl_3$, 300 MHz), (ppm): 8.69–8.67 (d, 1H), 8.60–8.53 (m, 3H), 8.46–8.45 (m, 2H), 8.24–8.19 (m, 3H), 8.10 (s, 1H), 7.97–7.69 (m, 12H), 7.63–7.59 (m, 3H), 7.53–7.40 (m, 7H), 7.27–7.21 (m, 2H), 4.22–4.20 (m, 4H), 2.17–2.08 (m, 2H), 1.44–1.35 (m, 16H), 1.01–0.93 (m, 12H). ^{13}C NMR ($CDCl_3$, 75 MHz) δ (ppm): 149.55, 147.12, 142.07, 140.45, 137.32, 133.59, 133.19, 132.64, 129.04, 128.23, 126.06, 125.69, 125.45, 123.85, 123.66, 123.38, 123.04, 121.83, 121.46, 121.22, 120.87, 119.19, 118.90, 117.54, 117.17, 109.31, 109.19, 39.38, 31.22, 30.45, 29.79, 28.67, 25.03, 22.98, 14.00, 10.77.

2.2.6. Iridium complexes

Cyclometalated Ir(III) chloro-bridged dimers of general formula $(CN)_2Ir(\mu\text{-}Cl)_2Ir(CN)_2$ (where CN represents a cyclometalating ligand) were synthesized by a previously reported method [32]. $IrCl_3.3H_2O$ was heated to 110 °C with 2.5 equivalent of cyclometalating ligand in a 3:1 mixture of 2-ethoxyethanol under argon for 24 h. The crude yields exceeded 85%. **Ir-1** and **Ir-2** were prepared according to a previous report [30].

Table 2
Contour plots of HOMOs and LUMOs of iridium dendrimers.

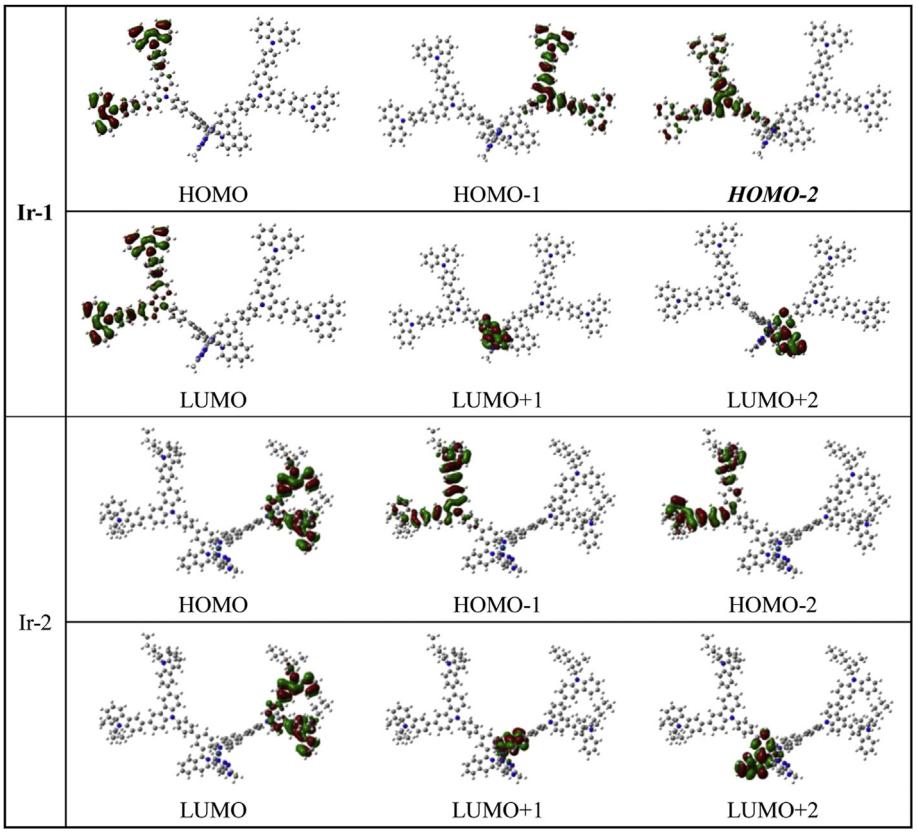

*2.2.7. Synthesis of **Ir-1***

The solution of 0.0726 g (0.45 mmol) 5-methyl-3-(pyridin-2′-yl)-1*H*-1,2,4-triazole and 0.122 g (2.25 mmol) sodium methoxide in 50 mL anhydrous ethanol was heated to 50 °C for 1 h. Up to 0.4502 g (0.11 mmol) of chloro-bridged dimer in 10 mL dichloromethane was dropped into the solution. The reacting mixture was refluxed for 3 h and cooled to room temperature. Water (50 mL) and dichloromethane (30 mL) were added, and then the organic layer was washed with water and dried with anhydrous magnesium sulfate. The mixture was purified by silica-gel column chromatography using acetone/dichloromethane (1/6) as eluent to yield a red powder (0.1631 g, isolated yield, 32.6%). MALDI-TOF: MH^+, 2207.8, ^{1}H NMR ($CDCl_3$, 300 MHz), (ppm): 9.19–9.14 (m, 2H), 8.67–8.58 (m, 7H), 8.35–8.34 (m, 1H), 8.20–8.14 (m, 9H), 8.00–7.61 (m, 35H), 7.55–7.46 (m, 22H), 7.35–7.25 (m, 10H), 7.17–7.15 (m, 2H), 6.70–6.65 (m, 2H), 2.53–2.51 (d, 3H). ^{13}C NMR ($CDCl_3$, 75 MHz) δ (ppm): 169.52, 169.27, 162.03, 157.92, 154.55, 152.63, 152.07, 149.83, 146.63, 142.26, 140.52, 138.13, 132.77, 131.47, 130.77, 130.25, 130.26, 129.10, 128.79, 127.50, 127.34, 127.02, 126.83, 126.38, 125.92, 125.45, 124.90, 124.17, 123.65, 122.98, 122.56, 121.10, 119.46, 119.14, 118.74, 113.65, 15.78. Calcd for $C_{146}H_{93}IrN_{12}$: C, 79.43; H, 4.25; Ir, 8.71; N, 7.61. Found: C, 79.25; H, 4.55; N, 7.82.

*2.2.8. Synthesis of **Ir-2***

The synthesis details of **Ir-2** are similar to those described for **Ir-1**. The crude product was separated by silica column chromatography using acetone/dichloromethane (1/6) as the eluent to yield a red powder (isolated yield 34.8%). MALDI-TOF: MH^+: 2352.2 (100%), ^{1}H NMR ($CDCl_3$, 400 MHz), (ppm): ^{1}H NMR δ ($CDCl_3$, 300 MHz), (ppm): 9.18–9.13(m, 2H), 8.67–8.48 (m, 11H), 8.24–8.22 (m, 5H), 7.93–7.83 (m, 26H), 7.65–7.63 (m, 5H), 7.53–7.43 (m, 15H), 7.28–7.25 (m, 4H), 6.68–6.63 (m, 2H), 4.24–4.19 (m, 8H), 2.54 (s, 3H), 2.19–2.15 (m, 4H), 1.45–1.28 (m, 32H), 1.00–0.89 (m, 24H). ^{13}C NMR ($CDCl_3$, 75 MHz) δ (ppm): 169.51, 163.22, 157.90, 155.06, 152.62, 149.76, 146. 84, 145.26, 142.18, 141.05, 137.83, 136.25, 136.41, 132.12, 131.24, 130.76, 130.52, 130.08, 128.98, 127.85, 127.36, 127.12, 126.27, 126.05, 125.38, 124.37, 121.54, 121.21, 121.05, 120.37, 119.43, 119.21, 118.55. 116.44, 47.65, 39.44, 31.26, 30.11, 29.69, 28.75, 24.62, 23.09, 15.78, 14.22, 10.89. Calcd for $C_{154}H_{141}IrN_{12}$: C, 78.64; H, 6.04; N, 7.15. Found: C, 79.01; H, 5.80; N, 6.86.

3. Results and discussion

3.1. Synthesis

The syntheses of the ligands and iridium dendrimers are shown in Schemes 1 and 2, respectively. The ligands and 5-methyl-3-(pyridin-2′-yl)-1*H*-1,2,4-triazole were synthesized according to literature [30]. The heteroptic complexes were prepared according to a two-step method as reported [30]. The Ir dimers were first synthesized, and then allowed to react with 3–5 equivalents of 5-methyl-3-(pyridin-2′-yl)-1*H*-1,2,4-triazole and an equivalent amount of sodium methoxide in ethanol at 50 °C for 3–5 h. All experiments involving Ir(III) species were carried out in inert atmosphere despite the good stability of the compounds in air. All the dendritic iridium complexes exhibited good solubility in common organic solvents and easily formed a uniform film by spin coating. The structures of the compounds were verified by ^{1}H NMR, GC–MS, and MALDI-TOF MS.

3.2. Electrochemistry

The electrochemical characteristics of the materials were investigated by CV methods (Fig. 1(a, b)). Solution CV measurements are fairly applicable to the discussion of energy levels in thin-film OLEDs [38]. The two dendrimers displayed two reversible oxidation waves. The relatively low oxidation potentials (E_{onset}) of 0.56 V for **Ir-1** and 0.70 V for **Ir-2** are ascribed to the mixture of the oxidation of Ir-*d* orbitals and ligands [39,40]. The Ir(1-piq)$_2$mpt (**G0**) was 0.97 V [30]. Thus, the peripheral dendrons and the 3,6-positions of the carbazole or 9-carbazole resulted in a cathodic shift of E_{ox1} because of the electronic effects of the peripheral carbazolyl-substituents at the cyclometalating ligand. E_{ox2} are ascribed to the oxidation of the peripheral carbazolyl-substituents. The first oxidation potentials were used to determine the HOMO energy levels. The energy level and energy gap

Table 3
Calculated HOMO and LUMO orbital energies and metallic d-orbital characteristics of iridium dendrimers at B3LYP/6–31G level.

	Occupied molecular orbitals			Unoccupied molecular orbitals		
		Energy (eV)	*d* (%)		Energy (eV)	*d* (%)
Ir-1	HOMO	−9.25	3.3	LUMO	−8.30	68.2
	HOMO−1	−9.12	0.5	LUMO+1	−6.12	4.4
	HOMO−2	−8.57	4.3	LUMO+2	−6.01	4.3
Ir-2	HOMO	−8.90	2.1	LUMO	−8.23	67.9
	HOMO−1	−9.06	0.4	LUMO+1	−6.26	4.6
	HOMO−2	−9.09	4.0	LUMO+2	−6.15	4.2

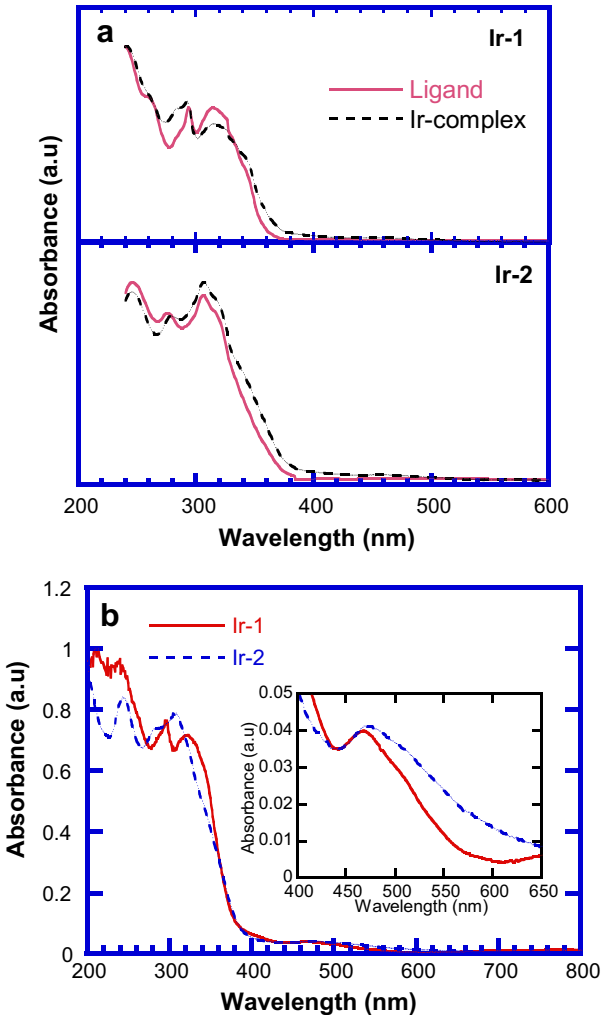

Fig. 2. UV–vis absorption spectra of the ligands and dendrimers in CH_2Cl_2 (**a**) and film (**b**).

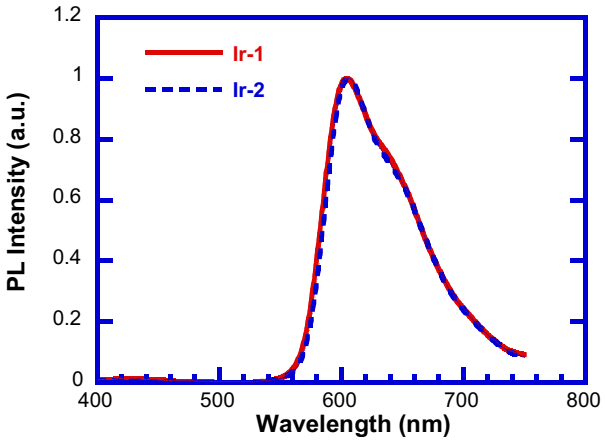

Fig. 3. PL spectra of **Ir-1** and **Ir-2** in CH_2Cl_2 solution.

were calculated with the empirical formula $E_{HOMO} = -e(E_{ox} + 4.40)$, $E_{LUMO} = -e(E_{re} + 4.40)$, $E_{gap} = E_{LUMO} - E_{HOMO}$ [41], which is based on an SCE energy level of 4.4 eV relative to the vacuum level. The HOMO energy levels were 4.96 eV for **Ir-1** and 5.10 eV for **Ir-2**. The E_{onset} values for the reductions were also at more negative potentials than **G0**. The data listed in Table 1 showed that the oxidation potential of Ir (III) decreased with increasing π-conjugation of the dendrons.

3.3. Theoretical calculations

On the basis of the optimized structures obtained by DFT methods, we investigated the d-orbital characteristics of the HOMOs and LUMOs of the Ir(III) dendrimers. The value of *d* indicates the electronic population of any electron localized on the centric Ir atoms, which is a criterion of the 7*d* or 8*d* characteristic of the orbital. The contour plots are listed in Table 2, and the results of the *d*-orbital characteristics are summarized in Table 3. The HOMOs and LUMOs were located at the ligand side and the composition of iridium was very low, indicating that the electronic transition

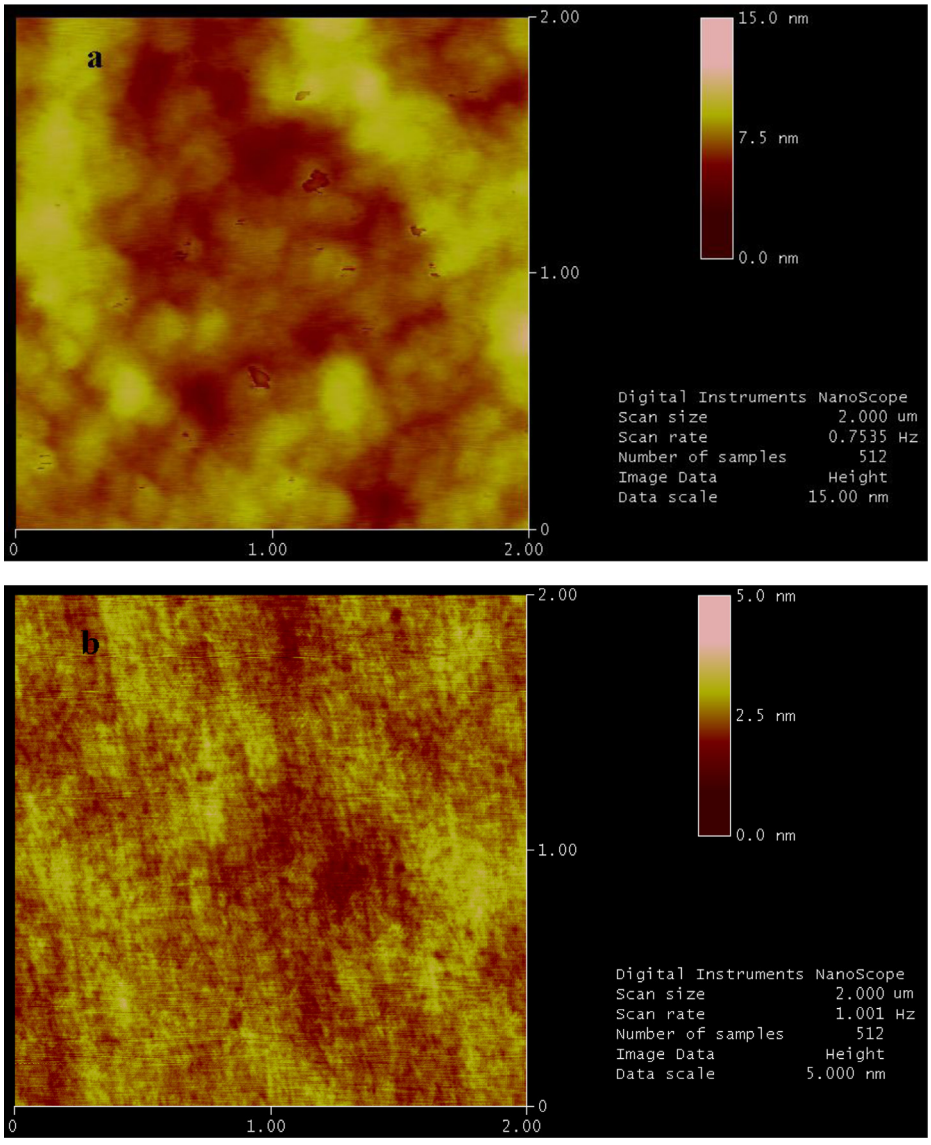

Fig. 4. The AFM images (2 μm × 2 μm) of **Ir-1** (a) and **Ir-2** (b) spin-coated in acetonitrile solution onto ITO substrates.

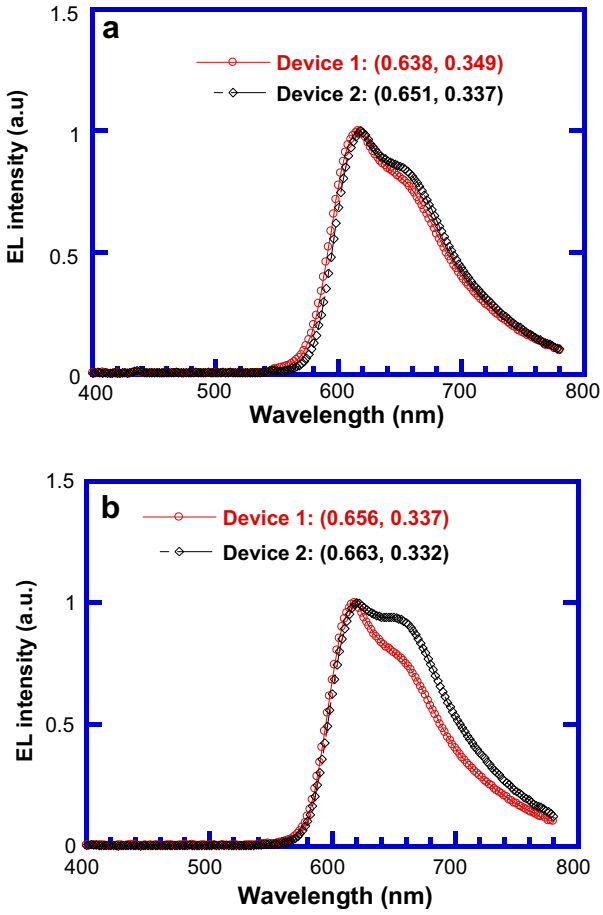

Fig. 5. EL spectra of device 1 and 2 for **Ir-1** (a) and **Ir-2** (b) obtained at a current density of 12 mA cm^{-2}.

between the orbitals occurs by predominant MLCT. The calculation of the electronic populations of the HOMOs and LUMOs predicted that strong MLCT transition will exist in the electronic transitions in the iridium dendrimers.

3.4. Photophysical properties

The UV–vis absorption of the obtained iridium(III) dendrimers and their ligands are depicted in Fig. 2 The dendrimers have three absorption bands from 240 to 320 nm in the UV region. These bands can be assigned to π–π^* transitions of the conjugated π-electron system of the corresponding ligand. **Ir-1** and **Ir-2** showed similar absorption bands to corresponding free ligands with minor red shifts in the CH_2Cl_2 solution. The MLCT absorption bands in the solution could not be clearly observed because of the strong absorption of the ligands. The weak and broad absorption bands longer than 400 nm in the film absorption (Fig. 2(b)) are assigned to ^{1}MLCT and ^{3}MLCT because of spin–orbit coupling.

Ir-1 and **Ir-2** showed similar PL spectra in the solution; the spectra peaked at 604 and 606 nm, respectively, which are red shifted by 11 and 13 nm from **G0** (Fig. 3). The PL spectra of both iridium (III) dendrimers blue shifted compared with those corresponding to homogeneous iridium complexes [5,29]. The absolute PL efficiencies of the neat films were measured in an integrating sphere under the 325 nm line of He–Cd laser. The values were 7.83% and 10.65% for **Ir-1** and **Ir-2**, respectively. The value for **G0** ($Ir(piq)_2mpz$) was 3.3%. The higher PL efficiency in **Ir-2** is associated with the bulky carbazolyl dendron attaching to the cores, which may suppress concentration quenching and reduce efficiency roll-off in OLEDs at high current density. Such effects are due to reduced triplet–triplet annihilation. The detailed photophysical properties are listed in Table 1.

AFM was used to characterize the surface morphologies of the light-emitting films. The phase images of the AFM studies obtained by tapping mode are shown in Fig. 4(a, b). Both iridium(III) dendrimers showed uniform film features. A more homogeneous film was observed for **Ir-2** with a root mean square roughness of 0.289 nm; the value for **Ir-1** was 1.058. The observation is in good agreement with the fact that 2-ethylhexyl linked in N-carbazolyl can improve the solubility of the dendrimer responsible for better surface morphology.

3.5. Electroluminescence performance

Ir-1 and **Ir-2** can be spin-coated to form high-quality thin films that are morphologically stable; thus, we fabricated host-free light-emitting devices using these compounds as single active components. To evaluate the influence of charge transport on device performance, three host-free types of devices with the configurations: (1) ITO/Dendrimer/TPBI/CsF/Al, (2) ITO/PEDOT/Dendrimer/TPBI/CsF/Al, (3) ITO/PEDOT/PVK/Dendrimer/TPBI/CsF/Al were fabricated and compared.

The EL spectra of polymer LEDs fabricated from **Ir-1** and **Ir-2** under different device configurations were obtained at a current density of 12 mA cm^{-2} (Fig. 5). The EL spectra recorded for the devices from iridium(III) dendrimers showed the same shape as the PL spectra measured in dichloromethane solution. The Commission Internationale De L'Eclairage coordinates of the devices listed in Table 4 were all in the saturated red region. The profile of the EL

Table 4
Device performance of iridium dendrimers with different device structures.

	Device	Device performance at maximal efficiency					J = 100 mA/cm^2				Brightness (cd/m^2)	Turn-on voltage[a] (V)	CIE (x, y)[b]
		Bias (V)	J (mA/cm^2)	L (cd/m^2)	QE (%)	L (cd/A)	Volt (V)	L (cd/m^2)	QE (%)	L (cd/A)			
Ir-1	1	12.6	7.4	191	3.6	2.6	18.6	1345	1.7	1.3	2289	8.0	0.638, 0.349
	2	10.9	4.2	140	5.1	3.3	15.8	1712	2.7	1.7	1712	7.7	0.651, 0.337
	3	14.9	1.8	60	5.1	3.3	21.6	1749	2.6	1.7	1992	11.3	0.655, 0.336
	4	10.8	0.3	11	5.7	4.4	22.9	1379	1.7	1.3	1658	9.5	0.641, 0.355
Ir-2	1	10.5	8.3	211	3.8	2.6	13.8	1715	2.5	1.7	2769	6.0	0.656, 0.337
	2	8.4	6.2	273	7.9	4.4	11.4	2443	4.3	2.4	3360	5.4	0.663, 0.332
	3	15.3	4.5	160	6.4	3.6	21.2	1927	3.5	2.0	3619	9.9	0.662, 0.332
	4	10.0	0.4	21.5	5.4	7.2	22.0	1523	2.0	1.5	1536	7.6	0.647, 0.348

Device structure: 1, ITO/Dendrimer/TPBI/CsF/Al; 2, ITO/PEDOT/Dendrimer/TPBI/CsF/Al; 3, ITO/PEDOT/PVK/Dendrimer/TPBI/CsF/Al; 4, ITO/PEDOT/Dendrimer + CBP(2:8)/TPBI/CsF/Al.

[a] At 1 cd/m^2.

[b] At maximal efficiency.

spectra of both iridium(III) dendrimers contained one peak at about 618 nm with a vibronic shoulder at 653 nm, coinciding very well with the PL spectrum (Fig. 3). The vibronic shoulders in devices 1 and 2, which are usually assigned to the excimer emission [42], were evident probably because of a facile formation of excimers in the devices.

The *J*–*L*–*V* characteristics of the obtained devices are shown in Fig. 6. All the EQEs reported in this work were corrected as commonly accepted IQEs [43]. Despite the absence of a hole-transporting layer, the iridium dendrimers were directly spin-cast onto the pre-cleaned ITO substrates from the solution in device 1, with moderate maximal EQEs of 3.6% and 3.8% for **Ir-1** and **Ir-2**, respectively. For device 2, a thin layer of PEDOT:PSS layer was incorporated as a hole-transporting layer between the emitting layer and ITO substrate. The efficiencies significantly increased for the devices based on both dendrimers. A maximal EQE of 5.1% and a luminous efficiency (LE) of 3.3 cd A^{-1} were recorded for the **Ir-1** device. The data were 7.9% and 4.4 cd A^{-1} for the **Ir-2** device. When the hole-transporting layer PVK was incorporated along the anode side, the maximal EQE for device 3 based on **Ir-1** and **Ir-2** were 5.1% and 6.4%, and the turn-on voltage raised from 7.7 V to11.3 V and 5.4 V to 9.9 V at 1 cd/m^2 respectively. The less efficient performance of the device 3 with PVK compared with that of device 2 fully revealed the hole transport characteristics of the iridium dendrimers.

To further elucidate the bipolar charge transport properties of the obtained dendrimers for both holes and electrons, we also compared the performance of device 2 (**Ir-1, Ir-2)** using 4,4-bis(carbazol-9-yl)biphenyl (CBP) as host material, which is recognized to be bipolar transporting with the same structure as the ITO/PEDOT/dendrimer (20 wt% in CBP)/TPBI/CsF/Al. Fig. 7(a, b) shows the *J*–*L*–*V* characteristics and QE–L–J of device 2 of the **Ir-2** and **Ir-2** based on the CBP host. At 120 cd m^{-2}, the EQE was 7.6% (at 7.80 V) for **Ir-2** and 6.4% (at 12.4 V) for **Ir-2**/CBP, suggesting that the dendrimers significantly contribute to charge transport. A peak EQE of 4.6% (2.56 cd m^{-2}) for **Ir-2** at a bias of 12.0 V at 100 mA cm^{-2} was achieved. The results revealed that the host-free devices without the host CBP exhibited better performance, and that large charge injection barriers or unbalanced carriers occurred. Such EL performance suggested that in the neat film configuration, electron and hole injections, as well as transport, were balanced, resulting in highly efficient charge capture inside the devices. The host-free devices showed better performance relative to the blend system. The detailed data were listed in Table 4.

The comparison of the HOMO energies of ITO and **Ir-1** and **Ir-2** indicated that the iridium dendrimers constituted a hole trap with depths of ca. 0.06 and 0.24 eV, respectively. The LUMO energies of **Ir-1** and **Ir-2** at −2.91 and −2.94 eV were only slightly lower than that of TPBI. Fig. 8 shows the work functions (ITO, 4.9 eV; PEDOT, 5.0 eV; PVK, 5.8 eV; CBP, 5.9 eV), which represent the extract transform load layer (TPBI, 2.70 eV; CsF, 2.2 eV) [44,45], suggesting that **Ir-1** and **Ir-2** acted as efficient bipolar transport materials. **Ir-1** and **Ir-2** had better hole injection and transport properties than did the electron. As indicated by AFM spectroscopy (Fig. 4), **Ir-2** exhibited a more uniform thin film than did **Ir-1**, which could be a contributing factor to the better performance of the former. Although the device performance needs further optimization, we

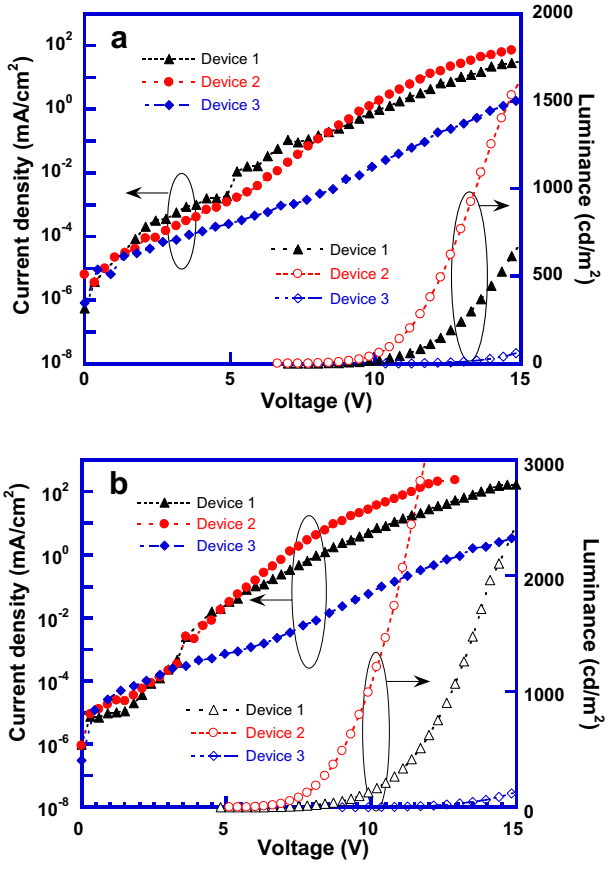

Fig. 6. The current density (*J*)–Voltage (*V*)–luminance (*L*) curves for **Ir-1** (a) and **Ir-2** (b)with different device structures: (1) ITO/dendrimer/TPBI/CsF/Al; (2) ITO/PEDOT/dendrimer/TPBI/CsF/Al; (3) ITO/PEDOT/PVK/dendrimer/TPBI/CsF/Al.

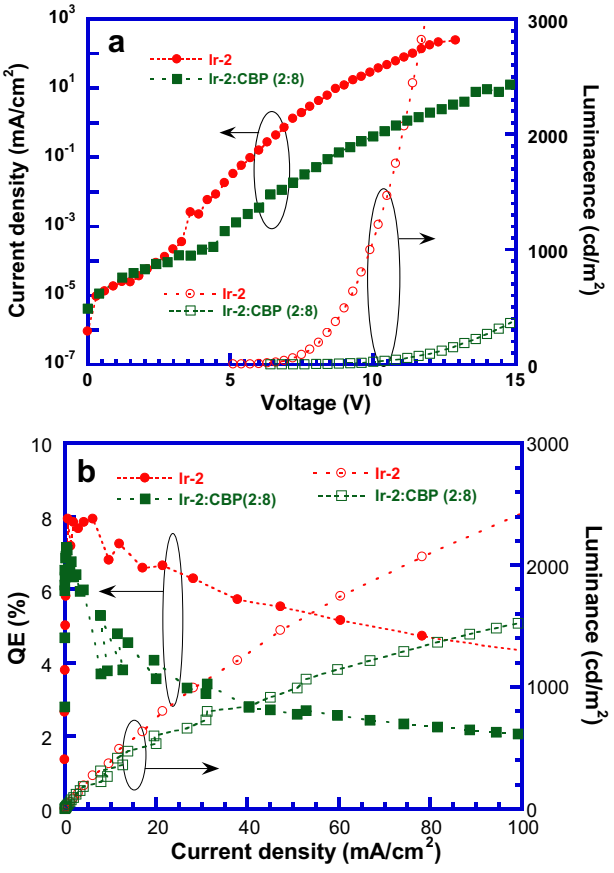

Fig. 7. The current density (*J*)–voltage (*V*)–luminance (*L*) characteristics of **Ir-2** (a), and luminance (*L*)–external quantum efficiency (*E*)–current density (*J*) of **Ir-2**(b) with different device structures: (1) ITO/PEDOT/Dendrimer/TPBI/CsF/Al, (2) ITO/PEDOT/(dendrimer:CBP(2:8))/TPBI/CsF/Al.

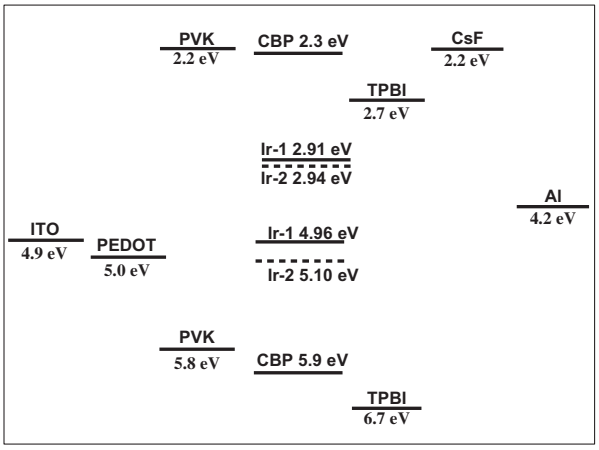

Fig. 8. Energy level diagram for the materials used in devices.

highlight the potential merits of this prominent class of iridium dendrimers in simplifying high-efficiency OLED applications.

4. Conclusion

An effective strategy for designing bipolar phosphorescent dendrimers has been demonstrated for electrophosphorescent devices. Introducing carbazolyl dendrons with excellent charge transport properties at the edge of the emissive core and 1,2,4-triazolyl unit moieties can significantly reduce the luminescence self-quenching caused by intermolecular interactions. A peak LE accompanied by high luminance was realized from a bilayer device. Surface groups play an important role in controlling solubility and intermolecular interactions, as indicated by the comparison of **Ir-1** and **Ir-2**. We believe that this strategy is suitable for the design and synthesis of novel solution-processable host-free phosphorescent materials and devices.

Acknowledgments

The authors sincerely appreciate the financial support given by the National Natural Science Foundation of China (gs1) (50803008), Natural Science Foundation of Hunan (gs2) (11B001, 2011RS4067), Open Project Program of Key Laboratory of Environmentally Friendly Chemistry & Applications of Ministry of Education (gs3) (08hjyh02), Key Laboratory for Power Technology of Renewable Energy Sources (gs4) (2011KFJJ006), the State Key Laboratory of Luminescent Materials and Devices at South China University of Technology (gs5) (2013-skllmd-08), China Postdoctoral Science Foundation (gs6) (20100480946, 201104508).

References

[1] Tang C, Van Slyke S. Organic electroluminescent diodes. Appl Phys Lett 1987;51:913–5.
[2] Burroughes J, Bradley DDC, Brown A, Marks R, Mackay K, Friend R, et al. Light-emitting diodes based on conjugated polymers. Nature 1990;347:539–41.
[3] Lo SC, Male NAH, Markham JPJ, Magennis SW, Burn PL, Salata OV, et al. Green phosphorescent dendrimer for light-emitting diodes. Adv Mater 2002;14:975–9.
[4] Chen ZQ, Bian ZQ, Huang CH. Functional Ir-III complexes and their applications. Adv Mater 2010;22:1534–9.
[5] Tsuboyama A, Iwawaki H, Furugori M, Mukaide T, Kamatani J, Igawa S, et al. Homoleptic cyclometalated iridium complexes with highly efficient red phosphorescence and application to organic light-emitting diode. J Am Chem Soc 2003;125:12,971–12,979.
[6] Huang YT, Chuang TH, Shu YL, Kuo YC, Wu PL, Yang CH, et al. Bi-substituted effect on phenylisoquinoline iridium(III) complexes. Organometallics 2005;24:6230–8.
[7] Zhu WG, Mo YQ, Yuan M, Yang W, Cao Y. Highly efficient electrophosphorescent devices based on conjugated polymers doped with iridium complexes. Appl Phys Lett 2002;80:2045–7.
[8] Jiang CY, Yang W, Peng JB, Xiao S, Cao Y. High-efficiency, saturated red-phosphorescent polymer light-emitting diodes based on conjugated and non-conjugated polymers doped with an Ir complex. Adv Mater 2004;16:537–41.
[9] Chen YC, Huang GS, Hsiao CC, Chen SA. High triplet energy polymer as host for electrophosphorescence with high efficiency. J Am Chem Soc 2006;128:8549–58.
[10] Xiao LX, Chen ZJ, Qu B, Luo JX, Kong S, Gong QH, et al. Recent progresses on materials for electrophosphorescent organic light-emitting devices. Adv Mater 2011;23:926–52.
[11] Chen LQ, You H, Yang CL, Zhang XW, Qin JG, Ma DG. Tuning the saturated red emission: synthesis, electrochemistry and photophysics of 2-arylquinoline based iridium(III) complexes and their application in OLEDs. J Mater Chem 2006;16:3332–9.
[12] Huang WS, Lin CW, Lin JT, Huang JH, Chu CW, Wu YH, et al. Highly branched green phosphorescent tris-cyclometalated iridium(III) complexes for solution-processed organic light-emitting diodes. Org Electron 2009;10:594–606.
[13] Zhu MR, Ye TL, He X, Cao XS, Zhong C, Ma DG, et al. Highly efficient solution-processed green and red electrophosphorescent devices enabled by small-molecule bipolar host material. J Mater Chem 2011;21:9326–31.
[14] Adachi C, Baldo MA, Thompson ME, Forrest SR. Nearly 100% internal phosphorescence efficiency in an organic light-emitting device. J Appl Phys 2001;90:5048–51.
[15] Tsuzuki T, Tokito S. Highly efficient, low-voltage phosphorescent organic light-emitting diodes using an iridium complex as the host material. Adv Mater 2007;19:276–80.
[16] Burn PL, Lo SC, Samuel IDW. The development of light-emitting dendrimers for displays. Adv Mater 2007;19:1675–88.
[17] Kwon TH, Kim MK, Kwon J, Shin DY, Park SJ, Lee CK, et al. Highly efficient light-harvesting system based on a phosphorescent acceptor coupled with dendrimer donors via singlet–singlet and triplet–triplet energy transfer. Chem Mater 2007;19:3673–80.
[18] Astruc D, Boisselier E, Ornelas C. Dendrimers designed for functions: from physical, photophysical, and supramolecular properties to applications in sensing, catalysis, molecular electronics, photonics, and nanomedicine. Chem Rev 2010;110:1857–959.
[19] Anthopoulos TD, Frampton MJ, Namdas EB, Burn PL, Samuel IDW. Solution-processable red phosphorescent dendrimers for light-emitting device applications. Adv Mater 2004;16:557–60.
[20] Lo SC, Namdas EB, Burn PL, Samuel IDW. Synthesis and properties of highly efficient electroluminescent green phosphorescent iridium cored dendrimers. Macromolecules 2003;36:9721–30.
[21] Lo SC, Harding RE, Brightman E, Burn PL, Samuel IDW. The development of phenylethylene dendrons for blue phosphorescent emitters. J Mater Chem 2009;19:3213–27.
[22] Markham JPJ, Samuel IDW, Lo SC, Burn PL, Weiter M, Bassler H. Charge transport in highly efficient iridium cored electrophosphorescent dendrimers. J Appl Phys 2004;95:438–45.
[23] Ribierre JC, Ruseckas A, Knights K, Staton SV, Cumpstey N, Burn PL, et al. Triplet exciton diffusion and phosphorescence quenching in iridium(III)-centered dendrimers. Phys Rev Lett 2008;100:017402.
[24] Ulbricht C, Beyer B, Friebe C, Winter A, Schubert US. Recent developments in the application of phosphorescent iridium(III) complex systems. Adv Mater 2009;21:4418–41.
[25] Chen LC, Ding JQ, Cheng YX, Xie ZY, Wang LX, Jing XB, et al. Bipolar heteroleptic green iridium dendrimers containing oligocarbazole and oxadiazole dendrons for bright and efficient nondoped electrophosphorescent devices. Chem Asian J 2011;6:1372–80.
[26] Lo SC, Anthopoulos TD, Namdas EB, Burn PL, Samuel IDW. Encapsulated cores: host-free organic light-emitting diodes based on solution-processible electrophosphorescent dendrimers. Adv Mater 2005;17:1945–8.
[27] Gambino S, Stevenson SG, Knights KA, Burn PL, Samuel IDW. Control of charge transport in iridium(III) complex-cored carbazole dendrimers by generation and structural modification. Adv Funct Mater 2009;19:317–23.
[28] Ding JQ, Wang B, Yue ZY, Yao B, Xie ZY, Cheng YX, et al. Bifunctional green iridium dendrimers with a "self-host" feature for highly efficient nondoped electrophosphorescent devices. Angew Chem Int Ed 2009;48:6664–6.
[29] Zhou GJ, Wong WY, Yao B, Xie ZY, Wang LX. Triphenylamine-dendronized pure red iridium phosphors with superior OLED efficiency/color purity trade-offs. Angew Chem Int Ed 2007;46:1149–51.
[30] Liang B, Wang L, Xu Y, Shi H, Cao Y. High-efficiency red phosphorescent iridium dendrimers with charge-transporting dendrons: synthesis and electroluminescent properties. Adv Funct Mater 2007;17:3580–9.
[31] Liang B, Jiang CY, Chen Z, Zhang XJ, Shi HH, Cao Y. New iridium complex as high-efficiency red phosphorescent emitter in polymer light-emitting devices. J Mater Chem 2006;16:1281–6.
[32] Orselli E, Kottas GS, Konradsson AE, Coppo P, Frohlich R, Frtshlich R, et al. Blue-emitting iridium complexes with substituted 1,2,4-triazole ligands: synthesis, photophysics, and devices. Inorg Chem 2007;46:11,082–11,093.
[33] Sonntag M, Kreger K, Hanft D, Strohriegl P, Setayesh S, de Leeuw D. Novel star-shaped triphenylamine-based molecular glasses and their use in OFETs. Chem Mater 2005;17:3031–9.
[34] Becke AD. Density-functional thermochemistry III. The role of exact exchange. J Chem Phys 1993;98:5648–52.

[35] Hay PJ, Wadt WR. Ab initio effective core potentials for molecular calculations. Potentials for K to Au including the outermost core orbitals. J Chem Phys 1985;82:299–310.
[36] Parr RG, Yang W. Density functional approach to the frontier-electron theory of chemical reactivity. J Am Chem Soc 1984;106:4049–50.
[37] Frisch MJ, Trucks GW, Schlegel HB, Scuseria GE, Robb MA, Cheeseman JR, et al. Gaussian 03, revision B. 05. Pittsburgh, PA: Gaussian Inc; 2003.
[38] Kulkarni AP, Tonzola CJ, Babel A, Jenekhe SA. Electron transport materials for organic light-emitting diodes. Chem Mater 2004;16:4556–73.
[39] Lamansky S, Djurovich P, Murphy D, Abdel-Razzaq F, Kwong R, Tsyba I, et al. Synthesis and characterization of phosphorescent cyclometalated iridium complexes. Inorg Chem 2001;40:1704–11.
[40] Li J, Djurovich PI, Alleyne BD, Yousufuddin M, Ho NN, Thomas JC, et al. Synthetic control of excited-state properties in cyclometalated Ir(III) complexes using ancillary ligands. Inorg Chem 2005;44:1713–27.
[41] Bredas J, Silbey R, Boudreaux D, Chance R. Chain-length dependence of electronic and electrochemical properties of conjugated systems: polyacetylene, polyphenylene, polythiophene, and polypyrrole. J Am Chem Soc 1983;105:6555–9.
[42] Yang C, Zhang X, You H, Zhu L, Chen L, Zhu L, et al. Tuning the energy level and photophysical and electroluminescent properties of heavy metal complexes by controlling the ligation of the metal with the carbon of the carbazole unit. Adv Funct Mater 2007;17:651–61.
[43] Forrest SR, Bradley DDC, Thompson ME. Measuring the efficiency of organic light-emitting devices. Adv Mater 2003;15:1043–8.
[44] Namdas EB, Anthopoulos TD, Samuel IDW, Frampton MJ, Lo SC, Burn PL. Simple color tuning of phosphorescent dendrimer light emitting diodes. Appl Phys Lett 2005;86:161104.
[45] Shirota Y, Kageyama H. Charge carrier transporting molecular materials and their applications in devices. Chem Rev 2007;107:953–1010.